Suplementary Information: On the Role of Topology in Regulating Transcriptional Cascades

Mahan Ghafari[1,2] and Alireza Mashaghi [1*]

[1]Leiden Academic Center for Drug Research, Faculty of Mathematics and Natural Sciences, Leiden University, Leiden, The Netherlands

[2]Department of Physics,Emory University,Atlanta,GA 30322, USA

August 9, 2017

Contents

A Finding the steady-state solution of a linear cascade

Consider the case of a linear cascade of arbitrary size, N: following equations (1) and (2) in the paper, we can write down the dynamics of each element in the cascade X_j using Hill function, except for the first element X_1 which has an inflow rate directly proportional to the expression level of the input signal S_x (only for mathematical convenience without loss of generality):

$$\begin{array}{rcll} \frac{dX_1}{dt} & = & S_x - \gamma X_1, & \\ \frac{dX_j}{dt} & = & \frac{V X_{j-1}^2}{X_{j-1}^2 + K^2} - \gamma X_j & (for\, j = 2, ..., N). \end{array} \tag{1}$$

*Alireza_a.mashaghi.tabari@lacdr.leidenuniv.nl

Assuming that the stimulus S_x is a Heaviside step function of magnitude β, i.e. $S_x(t) = \beta\theta(t)$, the steady-state solution can be found by solving the following set of coupled differential equations

$$\begin{array}{lll} \frac{dX_1^*}{dt} = S_x - \gamma X_1^* = 0 & \Rightarrow & X_1^* = \frac{\beta}{\gamma}, \\ \frac{dX_2^*}{dt} = \frac{V {X_1^*}^2}{{X_1^*}^2 + K^2} - \gamma X_2^* = 0 & \Rightarrow & X_2^*(\beta, K) = \frac{V}{\gamma}\left(\frac{\beta^2}{\beta^2 + K^2}\right), \\ . & & \\ . & & \\ \frac{dX_N^*}{dt} = \frac{V {X_{N-1}^*}^2}{X_{N-1}^{*2} + K^2} - \gamma X_N^* = 0 & \Rightarrow & X_N^*(\beta, K) = \frac{V}{\gamma}\left(\frac{X_{N-1}^{*2}(\beta,K)}{X_{N-1}^{*2}(\beta,K) + K^2}\right). \end{array} \tag{2}$$

Finding the steady-state values X_j^* is equivalent to finding the fixed points of a one-dimensional map $X_{j+1}^* = 1/\gamma\, A(X_j^*, K)$. Thus, the fixed points can be found

$$A(X^*, K) = \gamma X^* \quad \Rightarrow \quad X^* = \frac{V}{\gamma}\left(\frac{{X^*}^2}{{X^*}^2 + K^2}\right) \quad \Rightarrow \quad \begin{cases} X_{(1)}^* = & \frac{V + \sqrt{V^2 - 4\gamma^2 K^2}}{2\gamma} \\ X_{(2)}^* = & \frac{V - \sqrt{V^2 - 4\gamma^2 K^2}}{2\gamma} \\ X_{(3)}^* = & 0 \end{cases}. \tag{3}$$

By changing the parameter K for a fixed $V/(2\gamma)$, we have three possible scenarios (see figure S.1):
(i) $K > \frac{V}{2\gamma}$: One stable fixed point at $X^* = 0$.
(ii) $K = K_{crit} = \frac{V}{2\gamma}$: One stable fixed point at $X^* = 0$ and one saddle at $X^* = \frac{V}{2\gamma}$.
(iii) $K < \frac{V}{2\gamma}$: Two stable fixed points at $X^* = 0$ and $X^* = \frac{V + \sqrt{V^2 - 4\gamma^2 K^2}}{2\gamma}$, one unstable point at $X^* = \frac{V - \sqrt{V^2 - 4\gamma^2 K^2}}{2\gamma}$.

Thus, depending on the strength of the input signal β, degredation rate γ, maximum expression level V, and the value of K, the steady-state solution may converge to different stable points (see figure S.1).

B Linear cascade with one extra interaction at different positions

Now, we introduce an extra interaction of length one to the linear cascade at the transition point $K = K_{crit}$ (see the curved arrows in figure S.2a). We note that any extra interaction of length one is hypothetical since it implies that one element of the cascade is directly activating another element in two independent ways, i.e. one via the curved arrow and the other via the backbone linear sequence of activation, which might not be biologically meaningful, but serves as a mathematical tool to study the changes in the steady-state solution of the cascade in the presence of an extra interaction of minimal length. By changing the position of the curved arrow along the cascade, we

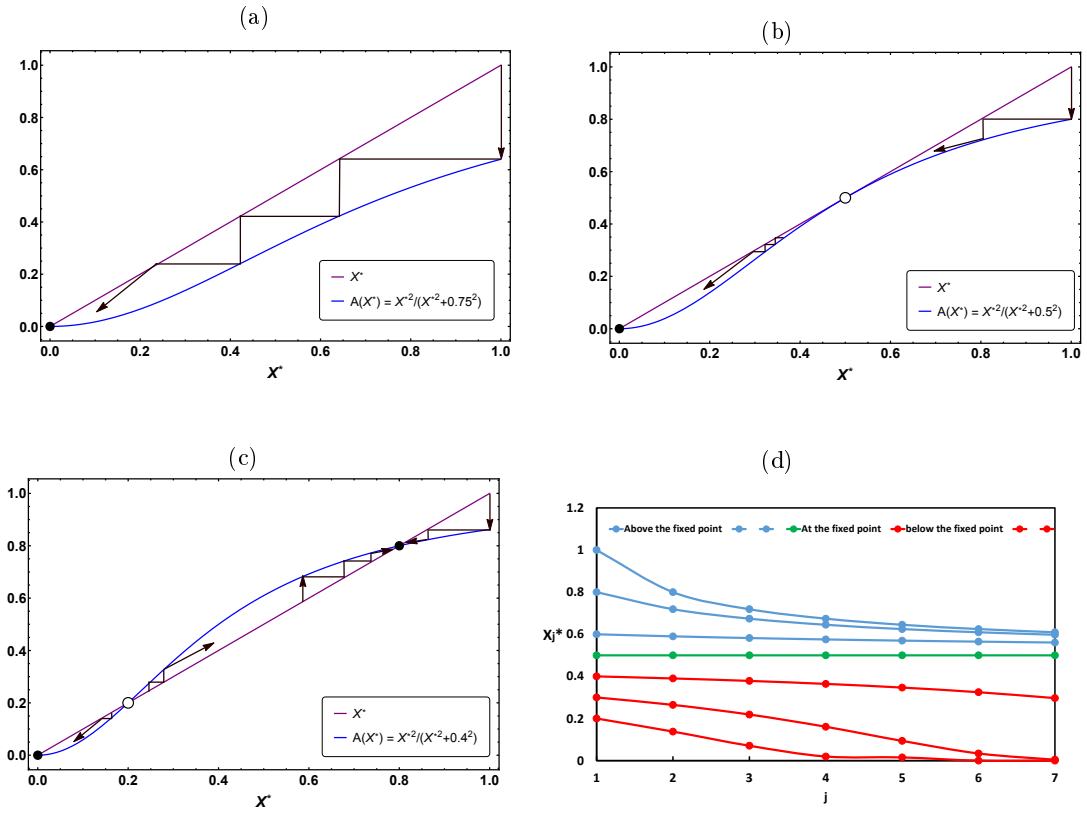

Figure S.1: Stability analysis of a linear signaling cascade with activating interactions (for the numerical results demonstrated, we set $\gamma = 1$). (a) When $K > K_{crit}$, there is only one stable fixed point at $X^*_{(3)} = 0$. Therefore, as the input signal is transmitting through the cascade, it will eventually die-out ($K = 0.75 > K_{crit} = 0.5$). (b) For $K = K_{crit}$, the system has one stable and one saddle points at $X^*_{(3)} = 0$ and $X^* = 0.5$, respectively. In this case, if the magnitude of the input is sufficiently high, i.e. $\beta \geq 0.5$, then the steady-state level of the output approaches $X^* = 0.5$. (c) When $K < K_{crit}$, the system has two stable fixed points at $X^*_{(3)}$, $X^*_{(1)}$, and one unstable point at $X^*_{(2)}$, respectively. If $\beta > X^*_{(2)}$, then the steady-state level of the output approaches its non-zero stable fixed point $X^*_{(1)}$ (in this plot $K = 0.45$). (d) The steady-state level of each element in the cascade (i.e. $j = 1, 2, \ldots, 7$) is demonstrated for the case of $K = K_{crit}$ (the lines are only for the guidance of the eye). The x-axis shows the j^{th} element of the cascade and the y-axis is the corresponding steady-state level. As demonstrated in part (b), if $\beta \geq 0.5$, then the input signal approach towards $X^* = 0.5$, otherwise it will die out eventually.

measure the half-life and steady-state response of the output as a function of curved arrow position. In order to explain the variations (see figures S.2c and S.2d), we demonstrate how the steady-state solution of the doubly interacting element X_m^* changes as the curved arrow is introduced into the cascade (see figure S.3).

As demonstrated in figure S.3, at the transition point $K = K_{crit}$, assuming the input signal has magnitude $\beta = 1$ and $V = 1$, the steady-state solution follows along the blue curve ${X^*}^2/({X^*}^2 + K_{crit}^2)$, except for the doubly interacting element X_3^* where it jumps towards the green or red curve (see figures S.3a and S.3b). Each time we apply the mapping function 3, it gives the steady-state solution of the next element until reaching the steady-state of the output X_N^*. When a repressing regulation of length one acts on X_3 (forming an incoherent feedforward loop between the two elements X_2 and X_3), it shifts the fixed point of the system to $X_{(3)}^* = 0$. That is why the steady-state of the output in figure S.2d decreases as we increase the length of the linear cascade N. However, in the case of a coherent feedforward loop between the two elements X_2 and X_3, the fixed point of the system does not shift and, consequently, the stead-state solution approaches to a non-zero value as demonstrated in S.2b. On the other hand, when we put the coherent feedforward loop further down the cascade, it shifts the fixed point. Consequently, the steady-states approach zero. Another interesting effect emerges from this system when the activating curved arrow acts on elements after the sixth element, i.e. $m \geqslant 7$. As it is demonstrated in figure S.2c, the steady-state values start to relax back to higher levels as the curved arrow gets closer to the end of the cascade. This occurs because the steady-state solution takes fewer steps before reaching the last element. In other words, in the case where m is close to N, the mapping function for the steady-state solution can be applied for fewer times, ultimately pushing the solution to higher values. A similar phenomenon explains the increasing trend in the steady-state of the output for a linear cascade with an incoherent feedforward loop in figure S.2d). We also note that the numerical results for the half-life time shows a decreasing trend for both the linear cascade with one incoherent feedforward loop and a cascade with a coherent feedforward loop for $m \geqslant 7$ (see figures S.2c and S.2e).

C Comparing the effect of topology on the steady-state solution

The critical dependency of steady-states on the type and position of the curved arrows lies on the changes that different circuit topologies bring to the steady-state solution of the doubly regulated elements of the cascade. In the case of one activating and one repressing extra interaction for CαI, i.e. the first curved arrow is an activating (A) and the second one is a repressing (R) Hill function (represented in figure S.4), for example, the effect of the three circuit topologies, with a fixed average contact order equal to 3, on the steady-state levels of the doubly regulated elements in the cascade can be calculated using the following set of equations:

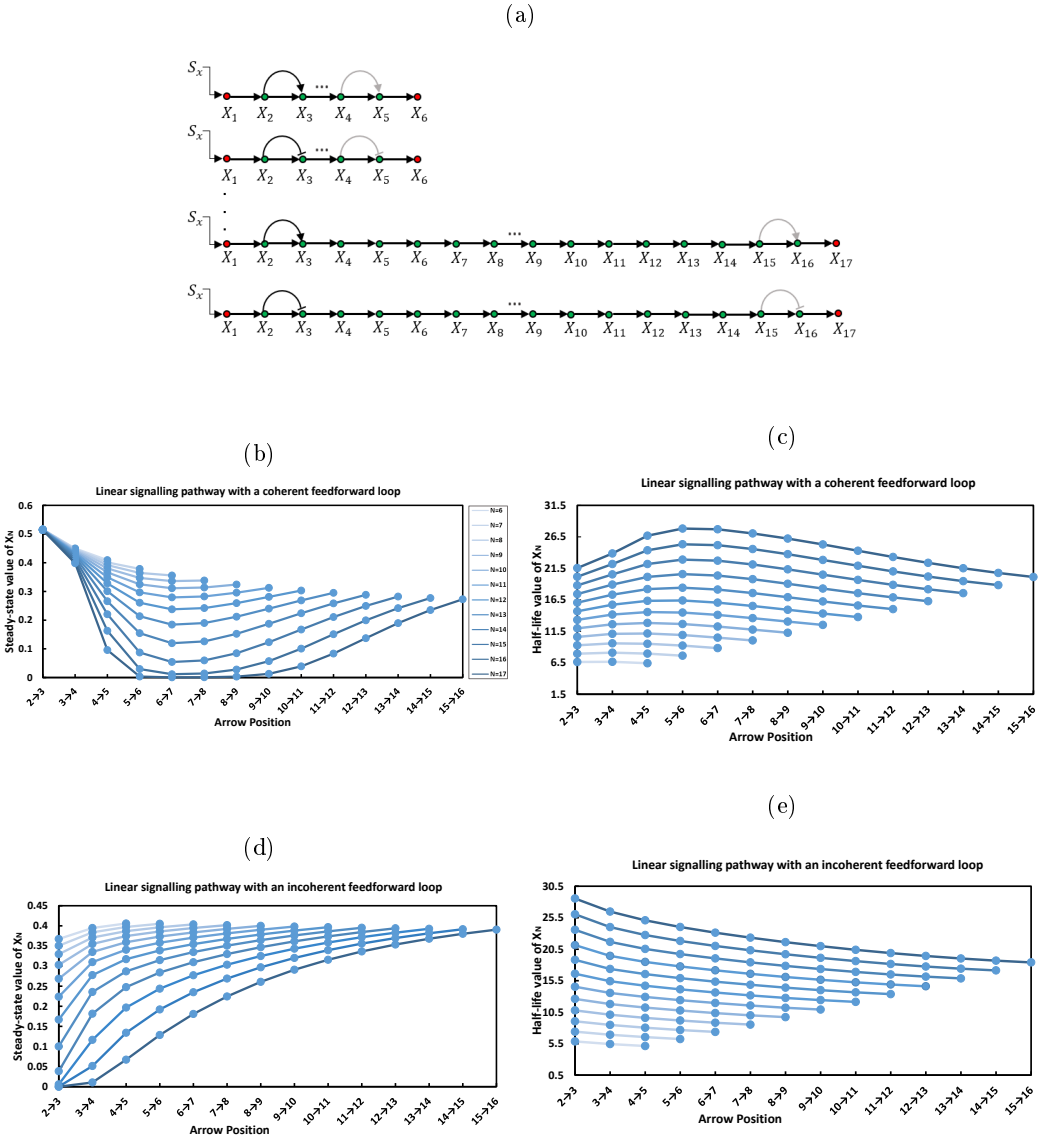

Figure S.2: The effect of a (in)coherent feedforward loop of length one in the response of a linear cascade is demonstrated. (a) Cascades of size $N = 6$ and $N = 17$ are demonstrated. An activating/reppressing curved arrow of length one is placed at different positions along the chain. The steady-state level and half-life time of the output is demonstrated as a function of (b) an activating curved arrow and (c) a repressing curved arrow. The numerical results are obtained for $\beta = 1$, $V/(2\gamma) = 1/2$, $K_{jA} = K_{crit} = 0.5$, and $K_R = 0.9$ (the lines are only drawn for the guidance of eye).

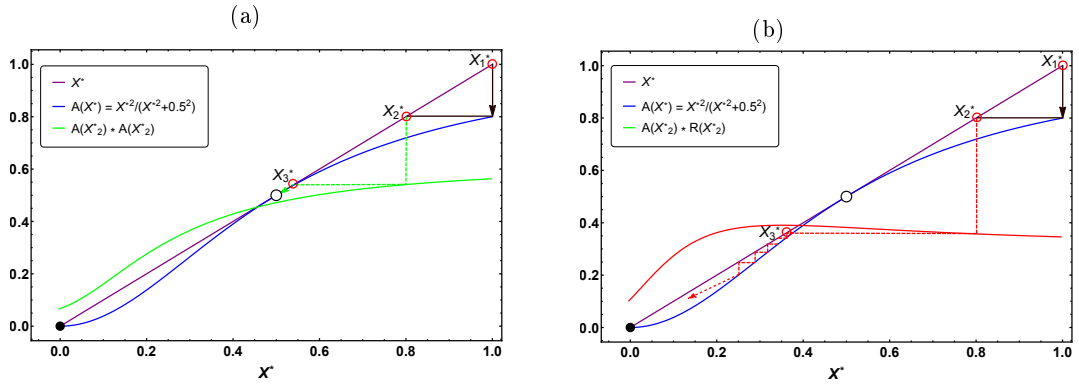

Figure S.3: Stability analysis of a linear cascade with one extra interaction of length one emerging from X_2 and acting on X_3. (a) An activating and (b) a repressing curved arrow of unit length is regulating X_3 and causes its steady-state level to decrease (green and red curves, respectively) from the expected steady-state solution of a linear cascade with no extra interaction (blue curve). In both cases, downstream elements proceeding X_3 should trace back the steady-state solution of the linear cascade (blue curve) as there are no further extra interaction in the cascade. In (a), since the extra activation does not cause the steady-state solution to jump over the fixed point$X^* = 0.5$, the steady-state level of the output $X_N^* \to 0.5$. If the magnitude of the input signal β is sufficiently smaller than 1, the curved arrow can shift the steady-state of X_3^* to drop below the fixed point $X^* = 0.5$. However, in (b), the repressing interaction pushes the steady-state solution below the fixed point and the steady-state level of the output, ultimately, approaches zero.

(i) For Cross configuration:

$$\begin{array}{rcl} X^*_m & = & A(X^*_{m-1}, K_A) \times A(X^*_{m-3}, K_A), \\ X^*_{m+2} & = & A(X^*_{m+1}, K_A) \times R(X^*_{m-1}, K_R), \end{array} \tag{4}$$

(ii) for Parallel configuration:

$$\begin{array}{rcl} X^*_m & = & A(X^*_{m-1}, K_A) \times A(X^*_{m-2}, K_A), \\ X^*_{m+1} & = & A(X^*_m, K_A) \times R(X^*_{m-3}, K_R), \end{array} \tag{5}$$

(iii) and for Series configuration:

$$\begin{array}{rcl} X^*_m & = & A(X^*_{m-1}, K_A) \times A(X^*_{m-3}, K_A), \\ X^*_{m+4} & = & A(X^*_{m+3}, K_A) \times R(X^*_{m+1}, K_R). \end{array} \tag{6}$$

The set of equations 4, 5, and 6 clarify how the steady-state of the doubly interacting elements depend on the type of interaction, circuit topology, and the position of the curved arrows. For a given set of reaction rates K, K_A, and K_R, the system can assume different fixed points (see figures S.4b, S.4c, and S.4d). Figure S.5 gives an overview of all possible circuit topologies with coherent and incoherent feedforward loops we considered in this paper.

D Time-dependent input signal

The method works as follows: Consider a coherent feedforward loop where X_1 activates X_2 and X_3, and X_2 activates X_3. Then, set the input signal to $S_x(t) = s_0(1 + \alpha sin(\omega t))$, and let the functions $h_1(X_1, S_x)$, $h_2(X_2, X_1)$, and $h_3(X_3, X_2, X_1)$ denote the net production rates for X_1, X_2, and X_3, respectively. Hence, we can write the dynamics for each element as the following:

$$\begin{array}{rcccl} \frac{dX_1}{dt} & = & h_1(X_1, S_x) & = & s_0(1 + \alpha sin(\omega t)) - \gamma X_1, \\ \frac{dX_2}{dt} & = & h_2(X_2, X_1) & = & A(X_1(t)) - \gamma X_2, \\ \frac{dX_3}{dt} & = & h_3(X_3, X_2, X_1) & = & A(X_2(t)) \times f_{cv}(X_1(t)) - \gamma X_3. \end{array} \tag{7}$$

Defining the deviations around the steady-state levels of each element to be $|\delta X_i| = X_i - X^*_i$ and $\delta S_x = S_x - s_{x_0}$, we assume that, to the first-order Taylor series expansion, they are small. Thus, we only keep the first leading terms in δX_i and δS_x:

$$\begin{array}{rcl} \frac{d\delta X_1}{dt} & = & g_1 \delta S_x + \omega_{c1} \delta X_1, \\ \frac{d\delta X_2}{dt} & = & g_{21} \delta X_1 + \omega_{c2} \delta X_2, \\ \frac{d\delta X_3}{dt} & = & g_{32} \delta X_2 + g_{31} \delta X_1 + \omega_{c3} \delta X_3, \end{array} \tag{8}$$

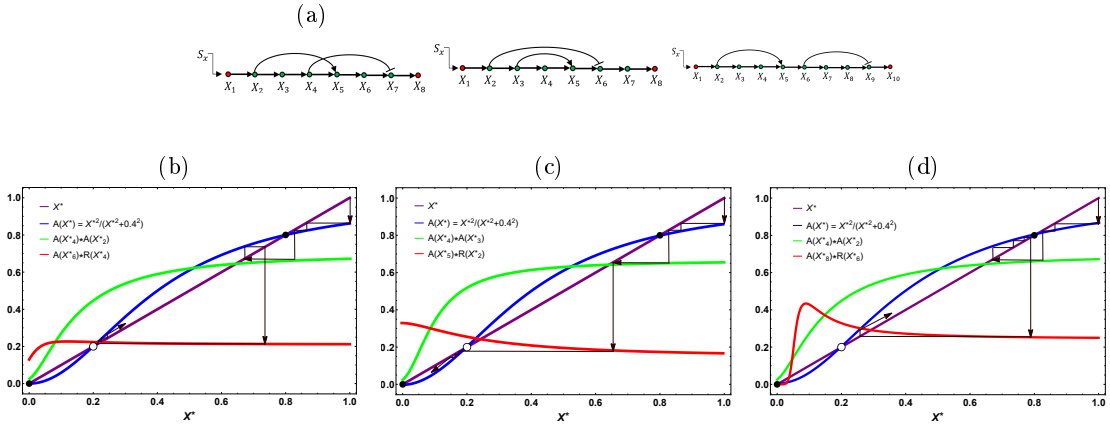

Figure S.4: (a) Three realizations of the CαI configuration (i.e. CXI, CPI, and CSI configurations from left to right, respectively, are demonstrated). (b) In this CXI realization, X_2 activates X_5 and X_4 represses X_7. While the two curved arrows push the steady-state value of X_7 to a very low amount, X_7^* is still bigger than the unstable fixed point at $X^* = 0.2$. Therefore, the steady-state values after X_7^* start to increase again by the activation interactions in the linear cascade and the input signal is restored. (c) In this CPI realization, X_3 activates X_5 and X_2 represses X_6 such that X_6^* becomes smaller than the unstable fixed point. Hence, the signal will die out eventually for the downstream elements. (d) In this CSI realization, after X_2 activates X_5, the remaining elements of the cascade can restore the input signal by the chain of activation interaction in the intermediate elements before X_6 represses X_9. Therefore, the decrease in the steady-state of X_9 is not big enough for the system to hop over the unstable fixed point and eventually approach to the non-trivial fixed point $X^* = 0.8$.

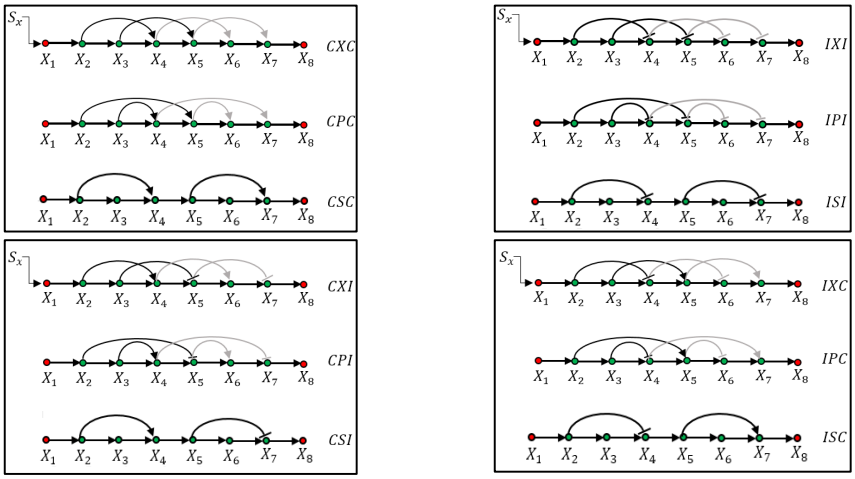

Figure S.5: Overview of cascades with different circuit topologies and constant contact order (CO=2).

where the gains and cut-off frequencies depend on the properties of the cascade

$$\begin{aligned}
g_1 &= \frac{\partial h_1(X_1,S_x)}{\partial S_x}\Big)_{(X_1^*,s_0)} &&= 1,\\
g_{21} &= \frac{\partial h_2(X_2,X_1)}{\partial X_1}\Big)_{(X_2^*,X_1^*)} &&= \frac{-2{X_1^*}^3}{(K_A^2+{X_1^*}^2)^2}+\frac{-2X_1^*}{K_A^2+{X_1^*}^2},\\
g_{32} &= \frac{\partial h_3(X_3,X_2,X_1)}{\partial X_1}\Big)_{(X_3^*,X_2^*)} &&= f_{cv}(X_1^*(t))\frac{\partial}{\partial X_2}(A_2(X_2))\Big)_{X_2^*},\\
g_{31} &= \frac{\partial h_3(X_3,X_2,X_1)}{\partial X_1}\Big)_{(X_3^*,X_1^*)} &&= A_2(X_2))_{X_2^*}\frac{\partial}{\partial X_1}(f_{cv}(X_1)),\\
\omega_{ci} &= \frac{\partial h_i}{\partial X_i}\Big)_{X_i^*} &&= -\gamma.
\end{aligned} \tag{9}$$

Solving the coupled differential equation 8, we find (for t large enough and $\omega \gg \omega_{c1},\omega_{c2},\omega_{c3}$):

$$\begin{aligned}
\delta X_1(t) &= -\tfrac{\alpha}{\omega^2+\omega_{c1}^2}\left[\omega_{c1}sin(\omega t)+\omega cos(\omega t)\right],\\
\delta X_2(t) &= -\tfrac{g_{21}\alpha}{(\omega^2+\omega_{c1}^2)(\omega^2+\omega_{c2}^2)}\big[\\
&\quad (\omega^2-\omega_{c1}\omega_{c2})sin(\omega t)-\omega(\omega_{c1}+\omega_{c2})cos(\omega t)\big],
\end{aligned} \tag{10}$$

$$\begin{aligned}
\delta X_3(t) = -\frac{1}{(\omega^2+\omega_{c2}^2)}\Bigg[&g_{31}\frac{\alpha\omega^2}{\omega^2+\omega_{c1}^2}sin(\omega t)+g_{32}g_{21}\\
&\frac{\alpha}{\omega^2+\omega_{c1}^2}\frac{\omega}{\omega^2+\omega_{c1}^2}(\omega(\omega_{c1}+\omega_{c2})cos(\omega t))\\
&-g_{31}(\omega_{c1}+\omega_{c2})\frac{\alpha\omega}{\omega^2+\omega_{c1}^2}cos(\omega t)+O\left(\frac{1}{\omega^2}\right)\Bigg].
\end{aligned} \tag{11}$$

Thus, in the limit of large input frequency, $\omega \gg \omega_{c1}, \omega_{c2}$, the amplitude of variation for each element in the feedforward loop can be simplified as:

$$\begin{aligned} |\delta X_1| &\propto \sqrt{\frac{\alpha^2}{\omega^2+\omega_{c1}^2}}, \\ |\delta X_2| &\propto \left(\frac{\alpha}{\omega^2+\omega_{c1}^2}\right)\left(\frac{g_{21}}{\omega^2+\omega_{c2}^2}\right)\omega^2, \\ |\delta X_3| &\propto \left(\frac{g_{31}}{\omega^2+\omega_{c1}^2}\right)\left(\frac{\alpha}{\omega^2+\omega_{c2}^2}\right)\omega^2. \end{aligned} \tag{12}$$